

See discussions, stats, and author profiles for this publication at: <https://www.researchgate.net/publication/41399726>

# The treatment of solid tumors by alpha emitters released from $^{224}\text{Ra}$ -loaded sources – Internal dosimetry analysis

Article in *Physics in Medicine and Biology* · February 2010

DOI: 10.1088/0031-9155/55/4/020 · Source: PubMed

CITATIONS

18

READS

370

5 authors, including:



L. Arazi

Ben-Gurion University of the Negev

109 PUBLICATIONS 1,540 CITATIONS

[SEE PROFILE](#)



Tomer Cooks

National Institutes of Health

28 PUBLICATIONS 933 CITATIONS

[SEE PROFILE](#)



Yona Keisari

Tel Aviv University

167 PUBLICATIONS 3,861 CITATIONS

[SEE PROFILE](#)



Itzhak Kelson

Tel Aviv University

135 PUBLICATIONS 1,610 CITATIONS

[SEE PROFILE](#)

Some of the authors of this publication are also working on these related projects:



Thymic humoral factor  $\gamma 2$  [View project](#)



Noble liquid radiation detectors; gas-avalanche detectors; internal potential emission detectors [View project](#)

The treatment of solid tumors by alpha emitters released from  $^{224}\text{Ra}$ -loaded sources—internal dosimetry analysis

This content has been downloaded from IOPscience. Please scroll down to see the full text.

2010 Phys. Med. Biol. 55 1203

(<http://iopscience.iop.org/0031-9155/55/4/020>)

View [the table of contents for this issue](#), or go to the [journal homepage](#) for more

Download details:

IP Address: 41.78.26.154

This content was downloaded on 14/10/2013 at 00:14

Please note that [terms and conditions apply](#).

## The treatment of solid tumors by alpha emitters released from $^{224}\text{Ra}$ -loaded sources—internal dosimetry analysis

L Arazi<sup>1,2,4</sup>, T Cooks<sup>3</sup>, M Schmidt<sup>1</sup>, Y Keisari<sup>3</sup> and I Kelson<sup>1,2,5</sup>

<sup>1</sup> School of Physics and Astronomy, Raymond and Beverly Sackler Faculty of Exact Sciences, Tel Aviv University, Tel Aviv 69978, Israel

<sup>2</sup> Althera Medical Ltd, Tel Aviv, Israel

<sup>3</sup> Department of Clinical Microbiology and Immunology, Sackler Faculty of Medicine, Tel Aviv University, Tel Aviv 69978, Israel

E-mail: [kelson@post.tau.ac.il](mailto:kelson@post.tau.ac.il)

Received 13 September 2009, in final form 30 December 2009

Published 2 February 2010

Online at [stacks.iop.org/PMB/55/1203](http://stacks.iop.org/PMB/55/1203)

### Abstract

Diffusing alpha-emitters radiation therapy (DART) is a proposed new form of brachytherapy, allowing the treatment of solid tumors by alpha particles. DART utilizes implantable sources carrying small activities of radium-224, which continually release into the tumor radon-220, polonium-216 and lead-212 atoms, while radium-224 itself remains fixed to the source. The released atoms disperse inside the tumor by diffusive and convective processes, creating, through their alpha emissions, a high-dose region measuring several mm in diameter about each source. The efficacy of DART has been demonstrated in preclinical studies on mice-borne squamous cell carcinoma and lung tumors and the method is now being developed toward clinical trials. This work studies DART safety with respect to the dose delivered to distant organs as a result of lead-212 leakage from the tumor through the blood, relying on a biokinetic calculation coupled to internal dose assessments. It is found that the dose-limiting organs are the kidneys and red bone marrow. Assuming a typical source spacing of  $\sim 5$  mm and a typical radium-224 activity density of  $0.4\text{--}0.8$  MBq  $\text{g}^{-1}$  of tumor tissue, it is predicted that tumors weighing up to several hundred grams may be treated without reaching the tolerance dose in any organ.

 This article has associated online supplementary data files

<sup>4</sup> Present address: Chemical Physics Department, Faculty of Chemistry, Weizmann Institute of Science, Rehovot 76100, Israel.

<sup>5</sup> Author to whom any correspondence should be addressed.

## 1. Introduction

Alpha particles, being a form of high linear energy transfer (LET) radiation, are highly effective against cancer cells. Their cell inactivation ability, usually requiring only a few hits to the nucleus, remains largely unchanged in hypoxic cells and is significantly less sensitive to dose rate and cell age variations than that of low-LET radiation (Barendsen *et al* 1966, Bedford and Mitchell 1973, Goodhead 1999, Hall 1994). In addition, the 50–100  $\mu\text{m}$  range of alpha particles in tissue may, in principle, guarantee that healthy tissue lying outside the target zone is spared.

The use of alpha radiation is presently investigated in preclinical settings and clinical trials as a means for treating malignancies characterized by single tumor cells in the circulation, micrometastases or microscopic cell clusters, utilizing monoclonal antibodies or peptides tagged with alpha emitters as targeting vectors (Allen 2006, Brechbiel 2007, Chérel *et al* 2006, Jurcic 2005, Kneifel *et al* 2006, Schmidt *et al* 2004). Such treatments, generally termed alpha-radioimmunotherapy, have—potentially—a higher therapeutic index than targeted therapies utilizing beta emitters. However, largely because of its short range, the treatment of solid tumors is widely considered to lie outside the scope of alpha-particle irradiation (Allen 2006, Couturier *et al* 2005, Kennel *et al* 1999, Mulford *et al* 2005, Zalutsky 2006).

In previous publications (Arazi *et al* 2007, Cooks *et al* 2008, 2009a, 2009b), we described a proposed new form of brachytherapy, which allows the treatment of solid tumors by alpha particles. The method, named diffusing alpha-emitters radiation therapy (DART), relies on the utilization of implantable radioactive sources which carry small activities of radium-224 ( $^{224}\text{Ra}$ , 3.7 days of half-life), incorporated into their surface. When  $^{224}\text{Ra}$  decays, it emits into the tumor its short-lived progeny: radon-220 ( $^{220}\text{Rn}$ , 55.6 s half-life), polonium-216 ( $^{216}\text{Po}$ , 0.15 s half-life) and lead-212 ( $^{212}\text{Pb}$ , 10.64 h half-life), which leave the source by virtue of their recoil energy. The released radionuclides spread by diffusive and convective processes in the vicinity of the source, leading to the formation of a continuous region of therapeutic high-LET dose through their alpha decays.  $^{220}\text{Rn}$  and  $^{216}\text{Po}$  contribute one alpha particle each (with respective energies of 6.29 MeV and 6.78 MeV).  $^{212}\text{Pb}$ , a pure beta emitter, gives rise to a third alpha particle (with an average energy of 7.80 MeV) through its daughter bismuth-212 ( $^{212}\text{Bi}$ , 60.6 min half-life) or granddaughter polonium-212 ( $^{212}\text{Po}$ , 0.30  $\mu\text{s}$  half-life).  $^{212}\text{Bi}$  either beta decays to  $^{212}\text{Po}$  with a branching ratio of 64.1%, or alpha decays to the pure beta emitter thallium-208 ( $^{208}\text{Tl}$ , 3.05 min half-life) with a branching ratio of 35.9%. The chain ends with stable  $^{208}\text{Pb}$ .

Preclinical work on mice-borne squamous cell carcinoma (SCC) and lung tumors, of both murine and human origin, has shown that each source leads to extensive cell death over a region measuring several mm in diameter (Arazi *et al* 2007, Cooks *et al* 2009b). Treatment of 6–7 mm diameter tumors by one or two sources was shown to result in pronounced tumor growth retardation (up to complete regression with no recurrence) and increased life expectancy, stemming from a decrease in lung metastases (Cooks *et al* 2008, 2009b). The efficacy of the method was further improved when combined with chemotherapy (Cooks *et al* 2009a).

The preclinical success of DART forms a strong motivation for its investigation in clinical settings. Indeed, preparatory work for a clinical study, focusing on late-stage head and neck SCC patients, is currently underway. This calls for a thorough consideration of the safety aspects of the proposed method.

In conventional radiotherapy, the tumor dose is, in many cases, limited by the need to avoid collateral damage to nearby tissue. In DART, however, it is anticipated that the rapid fall-off of the radiation field with the distance from the source will lead to a highly localized

tumor dose with minimal damage to adjacent healthy structures. Thus, the potentially limiting factor in DART is the dose delivered to distant organs as a result of radionuclide clearance from the tumor through the blood. This is the subject of the present work.

In principle, all of  $^{224}\text{Ra}$  progeny released from the DART sources may leave the tumor through the blood and redistribute throughout the body. However, because of the short half-lives of  $^{220}\text{Rn}$  and  $^{216}\text{Po}$ , it can be safely assumed that these two radionuclides decay entirely within the tumor.  $^{212}\text{Pb}$ , on the other hand, has a sufficiently long half-life to be partially taken out of the tumor, especially from well-vascularized regions that are more likely to be found near the tumor periphery, carrying with it its alpha-emitting daughters  $^{212}\text{Bi}$  and  $^{212}\text{Po}$ . As for  $^{224}\text{Ra}$ , the DART source production method limits the  $^{224}\text{Ra}$  activity which may be inadvertently shed from the source to a negligible fraction of the total source activity (less than about 0.5%). Thus, this effect is of little practical importance and will not be considered here.

This paper is organized as follows. We begin with a short survey of previously published preclinical results, which pertain to  $^{212}\text{Pb}$  leakage from DART-treated tumors and its subsequent uptake in distant organs. Noting the different macroscopic kinetics of lead in mice and man, we then turn to a theoretical approach based on established biokinetic models for lead and bismuth and the MIRD (Medical Internal Radiation Dose) scheme to estimate the organ dose in DART treatments to humans. The results of the combined biokinetic internal dose calculations are then compared to tolerance dose data to estimate the range of applicability of the DART method in terms of the maximal  $^{224}\text{Ra}$  activity which may be safely administered to human tumors.

## 2. Preclinical data

Preclinical data on murine SCC tumors (as well as on a wide range of other cell lines, as will be discussed in a separate publication) show that  $^{212}\text{Pb}$  indeed leaves the tumor through the blood and distributes throughout the body in varying concentrations (Arazi *et al* 2007). It was demonstrated that, for sources placed in the tumor center, the fraction of  $^{212}\text{Pb}$  activity leaving the tumor varies with tumor size, decreasing from 80–90% for small tumors ( $\sim 0.1$  g,  $\sim 4$ – $6$  mm diameter) to 10–15% in large tumors ( $\sim 2$  g, 15–20 mm diameter).  $^{212}\text{Pb}$  leaking from the tumors was found in all measured organs, in varying amounts which generally decreased with tumor mass. The largest  $^{212}\text{Pb}$  concentration was detected, in all cases, in the kidneys, followed by the liver, where the  $^{212}\text{Pb}$  concentration was about five times lower.  $^{212}\text{Pb}$  concentrations in other organs were lower by a factor of 10–100 compared to the kidneys. Blood samples taken from treated animals showed that the overall blood content of  $^{212}\text{Pb}$  was 1–7% of the entire  $^{212}\text{Pb}$  activity leaving the tumor, with more than 95% of the activity in the red blood cells (RBCs). Samples taken from adjacent tissue (in particular, the tumor bedding) contained minute  $^{212}\text{Pb}$  activities, with the same typical concentration found in other soft tissues (a few percent of the kidney concentration). Measurements of the activity ratio of  $^{212}\text{Bi}$  and  $^{212}\text{Pb}$  in DART-treated SCC tumors showed that the two nuclides are essentially in secular equilibrium throughout the tumor volume (activity ratio of  $1.0 \pm 0.1$ ).

## 3. Theoretical analysis

The biokinetics of lead in man is very different from that of mice. In particular, whereas in DART-treated mice the blood contains only a few percent of the total lead activity outside of the tumor, in humans  $\sim 55\%$  of intravenously injected lead is known to reside in the blood (Leggett 1993). Thus, in order to estimate organ doses in future DART treatments, we adopt

a theoretical approach, relying on established biokinetic models for humans. The preclinical data from mice thus serve to demonstrate that  $^{212}\text{Pb}$  indeed leaves the tumor through the blood, that the leaking fraction depends on the tumor size (or, more likely, on the distance between the source and vascularized regions near the tumor periphery) and that  $^{212}\text{Bi}$  and  $^{212}\text{Pb}$  are macroscopically close to secular equilibrium inside the tumor. The results of the biokinetic calculations (which pertain to  $^{212}\text{Pb}$ ,  $^{212}\text{Bi}$ ,  $^{212}\text{Po}$  and  $^{208}\text{Tl}$ ) are then used—following careful allocation of cumulated activities to specific organs—as an input to a dosimetric calculation based on the MIRD scheme (Stabin 2006).

### 3.1. Biokinetic model

Internal dosimetry estimates for DART rely on the age-specific biokinetic models for lead and bismuth developed by the International Commission on Radiological Protection (ICRP), based on an ensemble of data comprising experimental studies, long-term balance studies and autopsy measurements on humans and large animals (ICRP 1993, Leggett 1993). The model employed in the present work focuses on adults, but can be easily extended to all ages using the parameter values given in ICRP Publication 67 (ICRP 1993).

The compartments and transfer rates of the ICRP model were set by the commission (based on earlier work by Leggett (1993)) to reproduce the experimentally observed biokinetic behavior of lead, whose gross properties are as follows. Twenty-four hours after intravenous injection of radioactive lead into adult humans, the blood, liver, skeleton and kidneys contain, respectively, about 55%, 15%, 10–15% and 5% of the total lead activity in the body. Most of the remainder is associated with other soft tissue, with 3–6% excreted during the first day. Within several hours after injection, more than 99% of the lead activity in blood is associated with the RBCs, which return lead to the plasma with a half-time of a few days. Lead is lost from the liver and kidneys with apparent half-times of several weeks. A gradual loss of lead from the RBCs, liver and other soft tissues over the first few weeks can be accounted for by a slow release in urine and feces and a continual increase in skeletal lead (ICRP 1993).

Since dose delivery in DART is governed by the 3.7 days of half-life of  $^{224}\text{Ra}$  (75% of the dose is delivered within the first week), some of the transfer rates included in the ICRP model are too long to be of practical importance in this context. Thus, a simpler version of the ICRP model for lead was adopted, in which transfer routes for which the mean transfer time (the reciprocal of the transfer rate) was longer than 40 days were eliminated and some of the compartments and transfer routes were unified. The modified ICRP model is shown in figure 1, which also includes the values assigned to all transfer rates (in  $\text{d}^{-1}$ ). The major compartments in this model are the blood, skeleton, liver, kidneys and other soft tissues. The blood compartment is divided into plasma and RBCs. The skeleton is divided into cortical and trabecular bone compartments, each divided into a surface and volume sub-compartments (the division into exchangeable and non-exchangeable components included in the original ICRP model was discarded, because of the slow associated turnover rates). The liver and kidneys are each described as a single compartment (unlike the original ICRP model which includes two sub-compartments for both organs). The large soft tissue compartment is divided into two (rather than three) sub-compartments with different turnover rates (rapid/slow—denoted by STR and STS, respectively). The model includes lead transfer to and inside the gastrointestinal (GI) tract, here explicitly divided into the small intestine, upper and lower large intestines. Lead excretion through the urine, feces and sweat is described as in the ICRP model (excretion in hair and nails is too slow to be of importance for DART). In order to avoid unrealistic estimates concerning the dose to the urinary bladder wall, the model includes lead transfer from the urinary bladder contents to urine. When applied to DART, the results of the

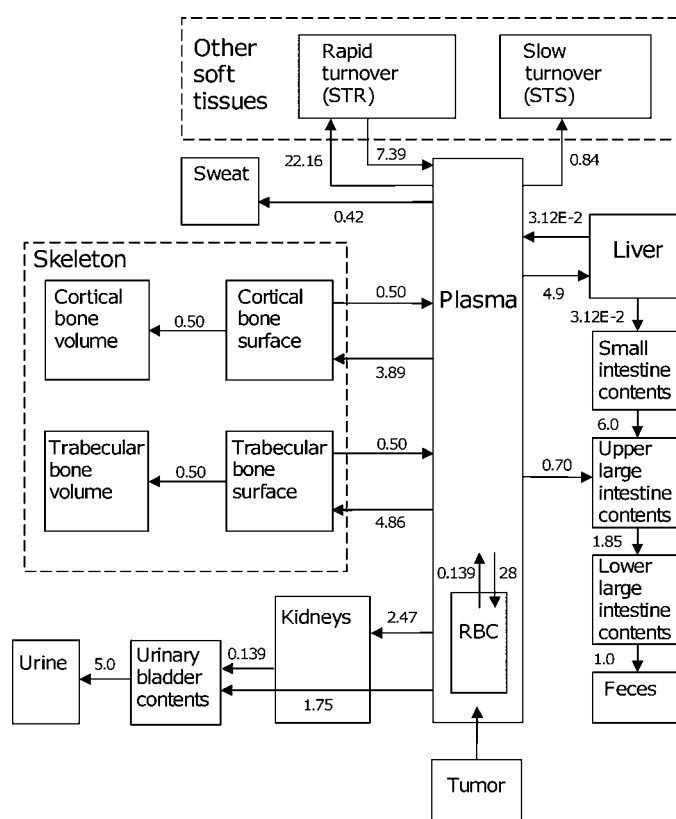


**Figure 1.** Block diagram of the biokinetic lead model, including the numerical values of the transfer rates (in  $\text{d}^{-1}$ ).

simplified version of the ICRP model (regarding the cumulated organ activities and doses) were found to be within 1% of those of the original ICRP model and within  $\sim 10\%$  of the original Leggett's model.

In order to simulate the temporal behavior of  $^{212}\text{Pb}$  uptake in the model compartments during the course of a DART treatment, the tumor is represented as a separate unit. The implanted  $^{224}\text{Ra}$  sources feed the tumor with  $^{212}\text{Pb}$ , which subsequently enters the blood at a rate that depends on the assumed  $^{212}\text{Pb}$  leakage probability  $P_{\text{leak}}$  (Pb) (the probability that a  $^{212}\text{Pb}$  atom released from the source decays outside of the tumor), as described in the appendix. For simplicity, we assume that the leakage probability—and hence the  $^{212}\text{Pb}$  clearance rate from the tumor—remains constant in time. We further assume that  $^{212}\text{Pb}$  leaves the tumor in the plasma. The model, described in detail in the appendix, is implemented by numerically solving a set of coupled first-order linear ordinary differential equations with constant coefficients, governing the exchange of lead between all compartments.

Because of the need to account for possible redistribution of  $^{212}\text{Bi}$  relative to  $^{212}\text{Pb}$  throughout the body, a biokinetic model for  $^{212}\text{Bi}$  is solved concurrently with that of  $^{212}\text{Pb}$ . This model, described mathematically in the appendix, relies on the assumptions made in ICRP Publication 67. Bismuth is removed from all tissues (other than bone volume) to the plasma at a rate of  $0.035 \text{ d}^{-1}$ . Of bismuth reaching the plasma, 35% goes to urine, 7% to the GI tract contents and subsequently to feces, 35% to the kidneys, 5% to the liver and 18% to

other tissues (see further division below). The total rate of removal from the plasma is  $50 \text{ d}^{-1}$ .  $^{212}\text{Bi}$  is generated by  $^{212}\text{Pb}$  decays in all compartments. Inside the bone volume, the  $^{212}\text{Bi}$  population is assumed to be governed by the decays of  $^{212}\text{Pb}$  and  $^{212}\text{Bi}$  itself with no exchange terms. Like  $^{212}\text{Pb}$ ,  $^{212}\text{Bi}$  leaving the tumor is also assigned to the plasma. For simplicity, the average clearance time of  $^{212}\text{Bi}$  from the tumor is assumed to be the same as that of lead. Note that since the preclinical data show that  $^{212}\text{Bi}$  is essentially in secular equilibrium with  $^{212}\text{Pb}$  inside the tumor, the average clearance time of bismuth from the tumor can be taken to be much longer than the  $^{212}\text{Bi}$  half-life (see the appendix). The  $^{212}\text{Bi}$  biokinetic model includes the same compartments as those of the simplified ICRP lead model, with the exception that the two soft tissue compartments are unified. Since the ICRP model for bismuth does not include specific reference to the transfer of bismuth from the kidneys to the urinary bladder contents, no such route is included in the model; rather,  $^{212}\text{Bi}$  is assumed to reach the urinary bladder contents directly from the plasma<sup>6</sup>. Transfer rates between the segments of the GI tract are assumed to be the same as in the lead model.

The ICRP did not address the question of bismuth exchange between the plasma and RBCs. Thus, as a working assumption, we take the transfer rate of bismuth from the RBCs to the plasma to be the same as that of lead, namely  $0.139 \text{ d}^{-1}$  (corresponding to a half-time of 5 days).  $^{212}\text{Bi}$  transfer from the plasma to the RBCs is assumed to be included in the 18% removed from the plasma to all tissues other than the urinary bladder, kidneys, liver and GI tract. The 18% is assigned as follows: 8.4% to RBCs (transfer rate  $4.22 \text{ d}^{-1}$ ), 6.9% to soft tissue ( $3.46 \text{ d}^{-1}$ ), 1.5% to the trabecular bone surface ( $0.73 \text{ d}^{-1}$ ) and 1.2% to the cortical bone surface ( $0.59 \text{ d}^{-1}$ ). The ratio between the transfer rates for these routes (which was not given by the ICRP) was taken, for simplicity, to be the same as for lead.

The two short-lived daughters of  $^{212}\text{Bi}$ ,  $^{212}\text{Po}$  and  $^{208}\text{Tl}$ , are assumed to be in secular equilibrium with their parent. Thus, their respective cumulated activities in each organ are 0.64 and 0.36 times that of  $^{212}\text{Bi}$ .

### 3.2. Allocation of cumulated activity to specific organs

Aside from the liver and kidneys, the biokinetic model does not relate to specific soft-tissue organs. In order to calculate the dose to all organs included in the MIRD scheme, it is necessary to allocate cumulated activities from the biokinetic model compartments to each individual organ. Allocation is made from the soft tissue compartment (based on the organ mass and estimated total soft tissue mass) and from the blood (based on the blood volume in each organ). Organ masses—as used in the OLINDA/EXM computer code (Stabin *et al* 2005)—were taken from Stabin and Siegel (2003) and blood volumes were taken from ICRP Publication 89 (ICRP 2002). Table S1 (in the supplementary online material available at [stacks.iop.org/PMB/55/1203/mmedia](http://stacks.iop.org/PMB/55/1203/mmedia)) lists the organs for which the dose is calculated (along with their contents where applicable), their masses and blood volumes (% of total blood). The total body mass was taken as 73.7 kg (as in OLINDA/EXM) and the total blood mass as 5.6 kg (ICRP 2002).

The total mass of soft tissue (excluding the liver and kidneys) was calculated by subtracting their masses, the mass of dry skeleton and teeth (5.2 kg), the total mass of blood (5.6 kg) and the mass of stomach contents (0.26 kg), GI tract contents (0.80 kg) and urinary bladder

<sup>6</sup> As noted above, the model includes two separate routes: one taking bismuth from the blood directly to the urinary bladder contents (neglecting the transit time through the kidneys) and the other from the blood to the kidneys without further transfer to urine. This is obviously an oversimplification, but the two routes work in opposite directions: the first tends to underestimate the kidney dose and the second to overestimate it. If one adopts the unrealistic assumption that all  $^{212}\text{Bi}$  atoms leaving the blood go to the kidneys and remain there, the kidney dose is increased by 22%.

contents (0.21 kg) from the total mass of the body (73.7 kg), giving  $M_{\text{ST}} = 59.4$  kg. For an organ of mass  $M_i$  (excluding the liver and kidneys), the cumulated activity of the  $k$ th isotope  $\tilde{A}_{k,i}$  was calculated by

$$\tilde{A}_{k,i} = \frac{M_i}{M_{\text{ST}}} \tilde{A}_{k,\text{ST}} + f_{\text{BV},i} \tilde{A}_{k,\text{blood}} \quad (1)$$

where  $f_{\text{BV},i}$  is the blood volume in the  $i$ th organ and  $\tilde{A}_{k,\text{ST}}$  and  $\tilde{A}_{k,\text{blood}}$  are the cumulated activities of the  $k$ th isotope in the soft tissue and blood compartments, respectively (for lead,  $\tilde{A}_{\text{Pb,ST}} = \tilde{A}_{\text{Pb,STR}} + \tilde{A}_{\text{Pb,STS}}$ ).  $\tilde{A}_{k,\text{blood}}$  is the sum of cumulated activities in the plasma and RBCs.

A few exceptions were dealt with differently. ICRP Publication 89 provides the blood volume for the stomach and esophagus together (1%). The blood volume allocated to the stomach wall was calculated as 1% times the mass of the stomach wall (158 g) divided by the sum of stomach wall mass and esophagus mass (40 g), giving 0.8%. Similarly, ICRP Publication 89 provides the blood volume of the entire large intestine (2.2%) without separating between its lower and upper parts (which are treated separately in the dosimetric calculation). The blood volumes for the walls of the upper and lower large intestine were calculated by their mass ratio, giving 1.25% for the former and 0.95% for the latter. The lungs are also treated in a special way. The total mass of the lungs (including blood) is given in Stabin and Siegel (2003) as 1.0 kg; of this  $\sim 0.5$  kg is contributed by the pulmonary blood. In order to allocate cumulated activity to the lungs, the net mass of lung tissue (0.5 kg) was used in equation (1), rather than 1 kg.

In the bone compartments, the red bone marrow, which, as discussed below, appears to be the dose-limiting organ (along with the kidneys), was allocated 4% of the blood plus a contribution from the soft tissue compartment based on its mass (in practice, the latter contribution to the total red marrow dose was found to be negligible compared to that arising from the blood). The cortical bone blood fraction (0.8%) was assigned to the cortical bone volume compartment (representing the blood vessels of the Haversian system). The trabecular bone blood fraction (1.2%) was assigned, as a conservative measure, to the trabecular bone surface compartment.

Organs for which the blood volume was not given in ICRP Publication 89 (breasts, ovaries, uterus, thymus and gall bladder wall) were assigned cumulated activities from the blood (more accurately, from the fraction contained in small vessels, which forms 56.5% of the total blood (ICRP 2002)), according to the ratio between their masses and the total soft tissue mass (soft tissue including the liver and kidneys).

### 3.3. Internal dose assessment

The dose to all organs is calculated by first setting the values for all input parameters: initial  $^{224}\text{Ra}$  activity administered to the tumor, effective  $^{212}\text{Pb}$  desorption probability from the source, average  $^{212}\text{Pb}$  leakage probability from the tumor and average clearance rate coefficient of  $^{212}\text{Bi}$  from the tumor (see the appendix for the exact definition of all parameters). Based on these values, the biokinetic calculation determines the cumulated activities of  $^{212}\text{Pb}$ ,  $^{212}\text{Bi}$ ,  $^{212}\text{Po}$  and  $^{208}\text{Tl}$  in all model compartments, which are then divided between all organs. The alpha, beta and gamma doses to all organs are subsequently calculated following the MIRD scheme. The alpha and beta doses given below were calculated using an indigenous computer code and compared to results obtained by the OLINDA/EXM 1.1 code. The gamma doses were calculated by OLINDA/EXM 1.1 only. For standard organs, the alpha and beta doses were calculated by assuming that the entire alpha-particle energy, or the average beta energy, is

deposited locally for each decay event (self-dose). For hollow organs, the dose to the wall was calculated by summing the self-dose of the wall and the contribution from the organ contents. The latter is given, according to the convention employed in the MIRD scheme, by

$$D_{\text{wall}} (\text{wall} \leftarrow \text{contents}) = f_c \frac{\tilde{A}_{\text{contents}} \times E}{2M_{\text{contents}}}. \quad (2)$$

For alpha particles a value  $f_c = 0.01$  was taken for the gall bladder, stomach, small and large intestines, while for the heart and urinary bladder wall a value  $f_c = 1$  was assumed, as in OLINDA/EXM 1.1 (Stabin 2009). For beta particles a value  $f_c = 1$  was taken for all hollow organs (Stabin and Siegel 2003).

Alpha-particle absorbed fractions (Stabin and Siegel 2003) for the bone targets, the red bone marrow (RM) and bone surface (BS, the 10  $\mu\text{m}$  layer of osteogenic cells on the bone surface), were taken from OLINDA/EXM 1.1, with two modifications: (1) the absorbed fraction for alpha particles irradiating the bone surface from the red marrow was taken as 0.09 for all energies (as in Stabin and Siegel (2003)) and (2) the absorbed fractions for  $^{212}\text{Po}$  were calculated by linear extrapolation to 8.79 MeV (OLINDA contains absorbed fractions for the range 3–8 MeV only). The absorbed fractions for beta particles were taken from Stabin and Siegel (2003). The values used in this work for alpha particles are given in table S2 (in the supplementary online material available at [stacks.iop.org/PMB/55/1203/mmedia](http://stacks.iop.org/PMB/55/1203/mmedia)).

### 3.4. Tolerance dose estimates

The practical range of applicability of DART, in terms of the total  $^{224}\text{Ra}$  activity that can be safely administered to the patient, will be limited by the need to prevent clinically detrimental non-stochastic tissue reactions (i.e., deterministic tissue injury such as kidney failure), which may appear either shortly after the treatment or within a few months or years<sup>7</sup>. In order to estimate the tolerated  $^{224}\text{Ra}$  activity, the calculated organ doses are combined with two additional data sets: a list of tolerance doses for all organs and a corresponding list of relative biological effectiveness (RBE) values. Tolerance doses were taken from ICRP Publication 41 (ICRP 1984). These correspond to the total gamma or x-ray doses, delivered in conventionally fractionated EBRT, that lead to tissue injury in 1–5% of the patients (a specific type of injury is considered for each organ, as detailed in table 2). RBE values for deterministic effects were taken from ICRP Publication 58 (ICRP 1989). The values used in the analysis are those corresponding to the limit of vanishingly small doses ( $\text{RBE}_m$ ), based on the linear-quadratic model (ICRP 1989). Note that the data in ICRP Publication 58 refer to *in vitro* and *in vivo* animal experiments (mice and hamsters) using heavy ion beams—carbon, neon and argon. For the purpose of the present analysis, the reference  $\text{RBE}_m$  values were taken for carbon ions beams with LET in the range 80–150 keV  $\mu\text{m}^{-1}$  (operated at a 4 cm spread Bragg peak). In the cases where  $\text{RBE}_m$  data were not available to the organ in question, the range 2–5 was adopted (being the observed range of  $\text{RBE}_m$  values for deterministic effects for heavy ions). The alpha-particle tolerance dose for each organ was estimated by dividing the organ x-ray tolerance dose by the corresponding value of  $\text{RBE}_m$ .

## 4. Results

Figure 2 shows the time-dependent  $^{212}\text{Pb}$  activity in the major compartments of the biokinetic model. The  $^{212}\text{Pb}$  leakage probability was taken as 30% and the effective  $^{212}\text{Pb}$  desorption

<sup>7</sup> As discussed below, because of risk/benefit considerations, the induction of secondary cancer does not play a role in determining the tolerance dose.

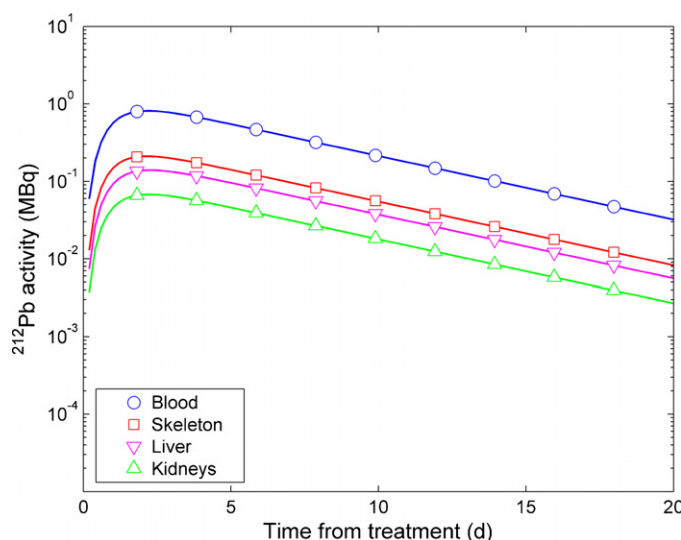


**Figure 2.** Results of the biokinetic calculation:  $^{212}\text{Pb}$  activity as a function of time in the blood, skeleton, liver and kidneys.

(This figure is in colour only in the electronic version)

probability was set at 0.55. The tumor was assumed to be a 4 cm diameter sphere with a specific density of  $1 \text{ g cm}^{-3}$ . Based on the preclinical observation that a source carrying a typical activity of  $\sim 50\text{--}200 \text{ kBq}$  (a few  $\mu\text{Ci}$ )  $^{224}\text{Ra}$  creates, in SCC tumors, a ‘kill region’ measuring  $\sim 5 \text{ mm}$  in diameter, we take, as a reference, a  $^{224}\text{Ra}$  activity density of  $0.37 \text{ MBq}$  ( $10 \mu\text{Ci}$ )  $\text{g}^{-1}$  of tumor tissue. For a 4 cm diameter spherical tumor, this translates to a total  $^{224}\text{Ra}$  activity of  $12.4 \text{ MBq}$  ( $335 \mu\text{Ci}$ ). The  $^{212}\text{Pb}$  activity in all organs reaches its maximal value about 2 days after treatment and is subsequently dominated by the exponential decay of  $^{224}\text{Ra}$ . For  $t > 2$  days, the blood holds 56% of the total  $^{212}\text{Pb}$  activity outside of the tumor, the skeleton 14%, liver 10%, kidneys 5% and all other soft tissues 9%. About 5% is excreted (4% in urine, 1% in sweat) and the remainder  $\sim 1\%$  is inside the GI tract contents or feces. Of lead residing in the blood, 95% are in the RBCs.

If one assumes that the removal time of bismuth from the tumor is the same as that of lead, the ratio of  $^{212}\text{Bi}$  to  $^{212}\text{Pb}$  cumulated activities inside the tumor is 0.96. With a  $^{212}\text{Pb}$  leakage probability of 30%, this translates to an average ratio of 1.09 between the  $^{212}\text{Bi}$  and  $^{212}\text{Pb}$  cumulated activities across all other compartments. In most organs, the ratio between the cumulated activities of  $^{212}\text{Bi}$  and  $^{212}\text{Pb}$  is close to the average (within a few percent). Exceptions are those organs for which the transfer rates from the plasma are much higher for bismuth than for lead, namely the kidneys ( $17.5 \text{ d}^{-1}$  compared to  $2.5 \text{ d}^{-1}$ ), urinary bladder contents ( $17.5 \text{ d}^{-1}$  compared to  $1.75 \text{ d}^{-1}$ ) and upper large intestine contents ( $3.5 \text{ d}^{-1}$  compared to  $0.7 \text{ d}^{-1}$ ). In all these organs, the  $^{212}\text{Bi}$  activity is significantly higher than that of  $^{212}\text{Pb}$ . As noted above, we adopt a working assumption, whereby the transfer rate of bismuth from the RBCs to the plasma is the same as that of lead (as well as the ratio between the bismuth transfer rates from the plasma to the RBCs and from the plasma to soft tissue). With these assumptions, the  $^{212}\text{Bi}/^{212}\text{Pb}$  cumulated activity ratios in the kidneys, urinary bladder contents and upper large intestine contents are 1.7, 3.5 and 1.8, respectively.

Table 1 shows the alpha, beta and gamma organ doses per one atom of  $^{212}\text{Pb}$  entering the circulation. As is evident from the table, for the organs receiving higher doses, the

**Table 1.** Calculated absorbed dose (Gy) per atom of  $^{212}\text{Pb}$  leaking out of the tumor through the blood. The alpha, beta and gamma components are shown separately.

Organ	Dose (Gy per $^{212}\text{Pb}$ atom entering the blood)		
	Alpha	Beta	Gamma
Adrenals	$2.8 \times 10^{-14}$	$3.1 \times 10^{-15}$	$2.3 \times 10^{-15}$
Brain	$8.1 \times 10^{-15}$	$9.1 \times 10^{-16}$	$5.8 \times 10^{-16}$
Breasts	$8.6 \times 10^{-15}$	$9.7 \times 10^{-16}$	$8.3 \times 10^{-16}$
Gall bladder wall	$8.9 \times 10^{-15}$	$4.5 \times 10^{-15}$	$2.6 \times 10^{-15}$
Lower large intestine wall	$4.2 \times 10^{-14}$	$7.7 \times 10^{-15}$	$1.5 \times 10^{-15}$
Small intestine wall	$4.1 \times 10^{-14}$	$4.7 \times 10^{-15}$	$1.6 \times 10^{-15}$
Stomach wall	$3.7 \times 10^{-14}$	$4.2 \times 10^{-15}$	$1.5 \times 10^{-15}$
Upper large intestine wall	$4.2 \times 10^{-14}$	$8.3 \times 10^{-15}$	$2.0 \times 10^{-15}$
Heart wall	$9.3 \times 10^{-14}$	$1.1 \times 10^{-14}$	$2.6 \times 10^{-15}$
Kidneys	$3.8 \times 10^{-13}$	$4.0 \times 10^{-14}$	$5.5 \times 10^{-15}$
Liver	$1.0 \times 10^{-13}$	$1.1 \times 10^{-14}$	$3.5 \times 10^{-15}$
Lungs	$8.8 \times 10^{-14}$	$9.9 \times 10^{-15}$	$1.7 \times 10^{-15}$
Muscle	$5.6 \times 10^{-15}$	$6.4 \times 10^{-16}$	$9.5 \times 10^{-16}$
Ovaries	$1.8 \times 10^{-14}$	$2.1 \times 10^{-15}$	$1.4 \times 10^{-15}$
Pancreas	$4.7 \times 10^{-14}$	$5.3 \times 10^{-15}$	$2.2 \times 10^{-15}$
Red marrow	$6.7 \times 10^{-14}$	$4.3 \times 10^{-15}$	$1.3 \times 10^{-15}$
Osteogenic cells	$2.2 \times 10^{-13}$	$8.4 \times 10^{-15}$	$1.3 \times 10^{-15}$
Skin	$1.3 \times 10^{-14}$	$1.4 \times 10^{-15}$	$5.9 \times 10^{-16}$
Spleen	$5.6 \times 10^{-14}$	$6.3 \times 10^{-15}$	$2.1 \times 10^{-15}$
Testes	$9.3 \times 10^{-15}$	$1.0 \times 10^{-15}$	$6.7 \times 10^{-16}$
Thymus	$8.6 \times 10^{-15}$	$9.7 \times 10^{-16}$	$1.2 \times 10^{-15}$
Thyroid	$8.6 \times 10^{-15}$	$9.7 \times 10^{-16}$	$7.1 \times 10^{-16}$
Urinary bladder wall	$1.0 \times 10^{-13}$	$1.0 \times 10^{-14}$	$2.2 \times 10^{-15}$
Uterus	$8.6 \times 10^{-15}$	$9.7 \times 10^{-16}$	$1.4 \times 10^{-15}$
Remainder of body	$1.1 \times 10^{-14}$	$1.2 \times 10^{-15}$	$2.2 \times 10^{-15}$

alpha-particle dose is typically one order of magnitude higher than the beta dose (which is usually, but not always, considerably larger than the gamma dose). Taking into account the higher RBE of alpha particles, the low-LET contributions are rather negligible. The calculated doses are relatively robust against changes in the (unknown) transfer rates of bismuth between the plasma and RBCs. For example, a tenfold increase in the transfer rate of bismuth from the RBCs to the plasma leads to a mere 10% increase in the kidney dose and 20% increase in the dose to the urinary bladder wall. In all other organs (including the large intestine), the dose *decreases* by 1–4% for the same change in model parameters.

Another important point regarding table 1 is that the doses are essentially independent of the assumed  $^{212}\text{Pb}$  leakage probability; changing  $P_{\text{leak}}$  (Pb) from 10% to 90% results in a 1–3% decrease in the dose (per one  $^{212}\text{Pb}$  atom leaving the tumor through the blood) in all organs, except for the kidneys (–14%) and urinary bladder wall (–32%) (these variations arise because bismuth is assumed to leave the tumor with the same clearance time as lead). Thus, the table can serve as a basis for calculating the dose for a wide range of leakage probabilities. Knowing the initial  $^{224}\text{Ra}$  activity,  $^{212}\text{Pb}$  desorption probability and (assumed)  $^{212}\text{Pb}$  leakage

**Table 2.** Estimated alpha-particle tolerance doses and organ doses for a specific example (4 cm tumor treated with 12.4 MBq  $^{224}\text{Ra}$  with 30%  $^{212}\text{Pb}$  leakage). The organs are sorted in ascending order based on the ratio between the tolerance dose and treatment dose. For each organ the table contains the following entries: (1) the clinical detrimental effect; (2) the gamma or x-ray dose causing the specified effect in 1–5% of the patients (in conventionally fractionated EBRT) (Gy); (3) the estimated value of  $\text{RBE}_m$ ; (4) the estimated alpha-particle tolerance dose (Gy); (5) the calculated alpha particle dose for the specific example in question; (6) the ratio between the estimated alpha-particle tolerance dose and treatment dose for this example.

Organ	Injury	X-ray tolerance dose (Gy)	$\text{RBE}_m$	Alpha tolerance dose (Gy)	Treatment alpha dose (Gy) 4 cm tumor	Tolerance dose/treatment dose
Kidneys	Nephrosclerosis	23	4–6	4–6	0.35	11–17
Red bone marrow	Hypoplasia	2	1.8–2.5	0.8–1.1	0.063	13–18
Ovaries	Permanent sterilization	2–3	2–5	0.4–1.5	0.017	24–88
Liver	Liver failure, ascites	35	2–5	7–18	0.094	75–190
Heart wall	Pericarditis, pancarditis	40	2–5	8–20	0.087	92–230
Testes	Permanent sterilization	5–15	2–5	1–7	0.009	110–780
Lungs	Pneumonitis, fibrosis	40	2–4	10–20	0.082	120–240
Urinary bladder wall	Ulcer, contracture	60	2–5	12–30	0.096	125–310
Lower large intestine wall	Ulcer, stricture	45	2.5	18	0.039	460
Upper large intestine wall	Ulcer, stricture	45	2.5	18	0.039	460
Small intestine wall	Ulcer, stricture	45	2.5	18	0.039	460
Adrenals	Hypoadrenalism	>60	2–5	12–30	0.026	460–1150
Stomach wall	Ulcer, stricture	45	2.5	18	0.035	510
Thyroid	Hypothyroidism	45	2–5	9–22	0.008	1130–2750
Breasts (female)	Atrophy and necrosis	>50	2–5	10–25	0.008	1250–3130
Brain	Necrosis	50	4	12	0.008	1500
Skin	Ulcer, severe fibrosis	55	3	18	0.012	1500
Uterus	Necrosis, perforation	>100	2–5	20–50	0.008	2500–6250
Muscle (skeletal)	Atrophy	>100	2–5	20–50	0.005	4000–10 000

probability, one can easily calculate the total number of  $^{212}\text{Pb}$  atoms entering the circulation and then use the table as a zero-order approximation for calculating the total dose to all organs.

Table 2 shows the calculated alpha-particle dose to all organs for the case of the 4 cm spherical tumor discussed above<sup>8</sup>. For each organ, the table contains the estimated alpha-particle tolerance dose (calculated from the known x-ray tolerance dose and estimated  $\text{RBE}_m$ ) and associated injury (for x-rays). As noted above the organ doses are relatively insensitive to changes in the unknown parameters of the model (namely the bismuth transfer rates inside the blood). The table shows that the kidneys and red bone marrow can be expected to be the dose-limiting organs. For this specific example, both organs receive a dose smaller by one order of magnitude than the tolerance dose. All other organs (except for the ovaries) are subject to doses two to three orders of magnitude smaller than the tolerance doses.

## 5. Discussion

The results presented in table 2 demonstrate that the tolerated  $^{224}\text{Ra}$  activity for DART treatments can be expected to be of the order of >100–200 MBq (a few mCi). As noted above, based on preclinical data regarding mice-borne SCC and lung tumors (of both murine and human origin), this corresponds to tumors weighing up to a few hundred grams, with

<sup>8</sup> The planned clinical trial will likely focus on smaller tumors.

a grid of sources spaced  $\sim 5$  mm apart. Obviously, DART treatments for well-localized tumors, weighing several dozen grams, can be expected to result in organ doses well below the tolerance levels.

The actual limit on tumor size will, of course, depend on the required  $^{224}\text{Ra}$  activity density inside the tumor. Variations in the recommended  $^{224}\text{Ra}$  activity density may arise from differences in the characteristic length scale characterizing the dispersion of  $^{224}\text{Ra}$  progeny atoms inside the tumor (which will probably be tumor-dependent), the degree of stochastic variations in the dose at a given distance from the source and the radiosensitivity of the tumor cells. Note that the  $^{224}\text{Ra}$  activity density required to achieve a given tumor dose level is highly dependent on the source spacing. In general, decreasing the source spacing allows for a significant reduction in the  $^{224}\text{Ra}$  activity density.

A key factor affecting the uptake of  $^{212}\text{Pb}$  in healthy organs is its average leakage probability from the tumor  $P_{\text{leak}}(\text{Pb})$ . While this parameter will not be known *a priori*, it can be expected to be of the order of a few dozen percent and to generally decrease with increasing tumor size.

The calculated dose in the red bone marrow depends on the assumed values for the absorbed fractions (table S2), which are model dependent. The absorbed fractions employed in the present work are those used by Stabin and Siegel (2003) (based on a model developed by K. Eckerman). A more recent work by Watchman *et al* (2005) shows that when the cellular structure of the bone marrow is taken into consideration and less conservative assumptions are adopted with respect to the location of alpha emitters inside the bone structure, the resulting absorbed fractions are lower by a factor of up to  $\sim 2$  relative to the Eckerman model. Thus, the actual bone marrow dose per  $^{212}\text{Pb}$  atom leaking from the tumor may be considerably lower than the values appearing in table 1. Furthermore, the actual values of the alpha-particle dose to other organs may also be lower than those given above, if one considers that a significant fraction of the alpha-particle energy emitted by blood-borne atoms remains in the blood. Further reduction in the dose to most organs may also result if one relaxes the assumption that all  $^{212}\text{Pb}$  atoms leave the tumor inside the plasma in an exchangeable form (i.e. in a chemical form that allows their transport out of the blood). In particular, some  $^{212}\text{Pb}$  atoms may leave the tumor bound either to the RBCs (which trap lead for several days) or to plasma proteins which are not exchangeable with other tissues (a feature included in the original Leggett's model).

The present analysis is purely theoretical in nature and should thus be considered as a rough guide for the design of clinical trials. In the course of such trials, which will apply a dose-escalating strategy, blood and urine samples will be routinely collected, providing valuable data on the actual rate of  $^{212}\text{Pb}$  leakage from the tumor and on the radiation response of the red bone marrow and kidneys.

As in all radiation treatments, there is some long-term risk of secondary-cancer induction in the case of DART. In particular, one should take into consideration the risk of long-term induction of kidney cancer (as the kidneys receive the highest dose in the course of DART treatments). However, at least initially, until considerable clinical experience with this new method is gained, DART will likely be employed in the treatment of terminal patients, for whom no other line of therapy may help. For such patients, the risk of secondary cancer induction will probably be of minor importance. With time, based on its performance in clinical trials, DART may potentially be used with curative intent (either as a stand-alone modality or in combination with other treatments, such as external beam radiation therapy), exploiting its ability to deliver therapeutic high-LET doses to radiation-resistant, hypoxic solid tumors without risking nearby structures. When such applications will be considered,

the question of potential long-term complications will have to be revisited and given the proper weight by the medical community.

A final note should be made with respect to the release of  $^{212}\text{Pb}$  from the tumor. The fact that the  $^{224}\text{Ra}$  decay chain ends with stable lead ( $^{208}\text{Pb}$ ) may suggest that DART treatments can result in lead toxicity. This concern can be addressed by analyzing the amounts of possibly released activity and corresponding masses involved. Suppose, for example, that a tumor is treated with 200 MBq of  $^{224}\text{Ra}$  (which is representative of the limit corresponding to the kidneys/red bone marrow tolerance dose). The total number of stable lead atoms released by all sources is  $\sim 5 \times 10^{13}$ , which is equivalent to a total lead mass of  $0.017 \mu\text{g}$ . The normal lead blood level is  $5 \mu\text{g dl}^{-1}$  (or a total of about  $250 \mu\text{g}$  in the blood only). Thus, even without considering lead atoms which normally reside outside of the blood, the additional stable lead resulting from a 200 MBq  $^{224}\text{Ra}$ , DART treatment will be  $\sim 1.5 \times 10^4$  times below the normal background.

### Acknowledgments

This work was performed in partial fulfillment of the requirements toward a PhD degree of LA and was partially supported by Althera Medical Ltd.

### Appendix

In what follows we describe in detail the mathematical model employed in the biokinetic calculation.

$^{212}\text{Pb}$  enters the tumor either by directly recoiling from the DART source (following the decay of  $^{216}\text{Po}$  below its surface) or through the decay of  $^{216}\text{Po}$  away from the source, following the recoil of either  $^{220}\text{Rn}$  or  $^{216}\text{Po}$  into the tumor. We denote by  $P_{\text{des}}^{\text{eff}}(\text{Pb})$  the effective desorption probability of  $^{212}\text{Pb}$  from the source, i.e. the probability that a  $^{212}\text{Pb}$  atom enters the tumor for each decay of  $^{224}\text{Ra}$  on the source (typically  $P_{\text{des}}^{\text{eff}}(\text{Pb}) = 0.5\text{--}0.6$ ). We denote by  $N_{\text{Ra}}^{\text{src}}(t)$  the number of  $^{224}\text{Ra}$  atoms on the source at time  $t$ , and by  $\Gamma_{\text{Ra}}^{\text{src}}(t) = \lambda_{\text{Ra}} N_{\text{Ra}}^{\text{src}}(t)$  the  $^{224}\text{Ra}$  activity on the source (with  $\lambda_{\text{Ra}}$  being the radioactive decay constant of  $^{224}\text{Ra}$ ). We denote by  $\alpha_{\text{Pb}}$  the average clearance rate coefficient of  $^{212}\text{Pb}$  from the tumor (the average time for  $^{212}\text{Pb}$  clearance is  $1/\alpha_{\text{Pb}}$ ). Neglecting the short transient of  $^{220}\text{Rn}$  and  $^{216}\text{Po}$  buildup inside the tumor (remembering that their respective half-lives are 55.6 s and 0.15 s), the temporal behavior of the number of  $^{212}\text{Pb}$  atoms inside the tumor,  $N_{\text{Pb}}^{\text{tum}}(t)$  is governed by

$$\frac{dN_{\text{Pb}}^{\text{tum}}}{dt} = P_{\text{des}}^{\text{eff}}(\text{Pb}) \Gamma_{\text{Ra}}^{\text{src}}(t) - (\lambda_{\text{Pb}} + \alpha_{\text{Pb}}) N_{\text{Pb}}^{\text{tum}} \quad (\text{A.1})$$

where  $\lambda_{\text{Pb}}$  is the radioactive decay constant of  $^{212}\text{Pb}$ . Since  $^{224}\text{Ra}$  remains fixed to the source,  $\Gamma_{\text{Ra}}^{\text{src}}(t) = \Gamma_{\text{Ra}}^{\text{src}}(0) e^{-\lambda_{\text{Ra}} t}$  ( $t = 0$  being the time of source insertion into the tumor). Furthermore, since the initial  $^{212}\text{Pb}$  activity inside the tumor is zero ( $\Gamma_{\text{Pb}}^{\text{tum}}(0) = \lambda_{\text{Pb}} N_{\text{Pb}}^{\text{tum}}(0) = 0$ ), we get

$$\Gamma_{\text{Pb}}^{\text{tum}}(t) = \frac{\lambda_{\text{Pb}}}{\lambda_{\text{Pb}} + \alpha_{\text{Pb}} - \lambda_{\text{Ra}}} P_{\text{des}}^{\text{eff}}(\text{Pb}) \Gamma_{\text{Ra}}^{\text{src}}(0) (e^{-\lambda_{\text{Ra}} t} - e^{-(\lambda_{\text{Pb}} + \alpha_{\text{Pb}}) t}) \quad (\text{A.2})$$

where we assumed, for simplicity, that  $\alpha_{\text{Pb}}$  is constant in time.

We define the  $^{212}\text{Pb}$  leakage probability  $P_{\text{leak}}(\text{Pb})$  as the probability that a  $^{212}\text{Pb}$  atom released from the source decays outside of the tumor. Equivalently, the leakage probability is the ratio between the number of  $^{212}\text{Pb}$  atoms leaking out of the tumor from source insertion

to infinity and the number of  $^{212}\text{Pb}$  atoms released by the source. Using equations (A.1) and (A.2) we find

$$P_{\text{leak}}(\text{Pb}) = \frac{\int_0^\infty \alpha_{\text{Pb}} N_{\text{Pb}}^{\text{tum}}(t) dt}{\int_0^\infty P_{\text{des}}^{\text{eff}}(\text{Pb}) \Gamma_{\text{Ra}}^{\text{src}}(t) dt} = \frac{\alpha_{\text{Pb}}}{\alpha_{\text{Pb}} + \lambda_{\text{Pb}}}. \quad (\text{A.3})$$

$^{212}\text{Pb}$  leaving the tumor is assigned to the plasma. Thus, the  $^{212}\text{Pb}$  population in the plasma is governed by

$$\frac{dN_{\text{Pb,PL}}}{dt} = \sum_j \omega_{\text{Pb}}(j \rightarrow \text{PL}) N_{\text{Pb},j} - \left( \sum_j \omega_{\text{Pb}}(\text{PL} \rightarrow j) \right) N_{\text{Pb,PL}} - \lambda_{\text{Pb}} N_{\text{Pb,PL}} + \alpha_{\text{Pb}} N_{\text{Pb}}^{\text{tum}} \quad (\text{A.4})$$

where  $N_{\text{Pb},i}(t)$  is the total number of  $^{212}\text{Pb}$  atoms in the  $i$ th compartment at time  $t$  and  $\omega_{\text{Pb}}(i \rightarrow j)$  is the lead transfer rate from compartment  $i$  to compartment  $j$ . Note the inclusion of the radioactive decay term  $\lambda_{\text{Pb}} N_{\text{Pb},i}$ . For all other compartments, the equations take the form

$$\frac{dN_{\text{Pb},i}}{dt} = \sum_j \omega_{\text{Pb}}(j \rightarrow i) N_{\text{Pb},j} - \left( \sum_j \omega_{\text{Pb}}(i \rightarrow j) + \lambda_{\text{Pb}} \right) N_{\text{Pb},i}. \quad (\text{A.5})$$

Inside the tumor, the bismuth population is governed by

$$\frac{dN_{\text{Bi}}^{\text{tum}}}{dt} = \lambda_{\text{Pb}} N_{\text{Pb}}^{\text{tum}} - (\lambda_{\text{Bi}} + \alpha_{\text{Bi}}) N_{\text{Bi}}^{\text{tum}} \quad (\text{A.6})$$

with similar notation as equation (A.1). Note that  $^{212}\text{Bi}$  is assumed to enter the tumor only as the decay product of  $^{212}\text{Pb}$  outside the source, with no contribution made by direct recoil from the source itself. This is a valid assumption, since the maximum recoil energy imparted to  $^{212}\text{Bi}$  in the beta decay of  $^{212}\text{Pb}$  is 1.46 eV. This limits the direct desorption of  $^{212}\text{Bi}$  from the source to  $^{212}\text{Pb}$  atoms residing on the outermost layer of the source surface, which constitute a negligible fraction of the total  $^{212}\text{Pb}$  population on the source. Preclinical data from mice tumors (Arazi *et al* 2007) show that the activity ratio of  $^{212}\text{Bi}$  to  $^{212}\text{Pb}$  inside the tumor is  $1.0 \pm 0.1$ , implying that  $\alpha_{\text{Bi}}$  is significantly smaller than  $\lambda_{\text{Bi}}$ . The equation governing the  $^{212}\text{Bi}$  population in the plasma is

$$\frac{dN_{\text{Bi,PL}}}{dt} = \sum_j \omega_{\text{Bi}}(j \rightarrow \text{PL}) N_{\text{Bi},j} - \left( \sum_j \omega_{\text{Bi}}(\text{PL} \rightarrow j) \right) N_{\text{Bi,PL}} + \lambda_{\text{Pb}} N_{\text{Pb,PL}} - \lambda_{\text{Bi}} N_{\text{Bi,PL}} + \alpha_{\text{Bi}} N_{\text{Bi}}^{\text{tum}}. \quad (\text{A.7})$$

In all other compartments (other than bone volume),

$$\frac{dN_{\text{Bi},i}}{dt} = \lambda_{\text{Pb}} N_{\text{Pb},i} + \sum_j \omega_{\text{Bi}}(j \rightarrow i) N_{\text{Bi},j} - \left( \sum_j \omega_{\text{Bi}}(i \rightarrow j) + \lambda_{\text{Bi}} \right) N_{\text{Bi},i}. \quad (\text{A.8})$$

In the bone volume compartments,

$$\frac{dN_{\text{Bi},i}}{dt} = \lambda_{\text{Pb}} N_{\text{Pb},i} - \lambda_{\text{Bi}} N_{\text{Bi},i}. \quad (\text{A.9})$$

The final outcome of the biokinetic calculation for  $^{212}\text{Pb}$  and  $^{212}\text{Bi}$  is the total number of decays (cumulated activities) of both nuclides in each of the model compartments:  $\tilde{A}_{\text{Pb},i}$  and  $\tilde{A}_{\text{Bi},i}$ ,

where

$$\tilde{A}_{k,i} = \int_0^{\infty} \lambda_k N_{k,i}(t) dt. \quad (\text{A.10})$$

The total number of decays of  $^{212}\text{Po}$  and  $^{208}\text{Tl}$  in each compartment is taken as 0.64 and 0.36 times that of  $^{212}\text{Bi}$ , respectively (reflecting the respective branching ratios of  $^{212}\text{Bi}$  decay),  $\tilde{A}_{\text{Po},i} = 0.64\tilde{A}_{\text{Bi},i}$ ,  $\tilde{A}_{\text{Tl},i} = 0.36\tilde{A}_{\text{Bi},i}$ .

## References

- Allen B J 2006 Internal high linear energy transfer (LET) targeted radiotherapy for cancer *Phys. Med. Biol.* **51** R327–41
- Arazi L, Cooks T, M, Keisari Y and Kelson I 2007 Treatment of solid tumors by interstitial release of recoiling short-lived alpha emitters *Phys. Med. Biol.* **52** 5025–42
- Barendsen G W, Koot C J, Van Kersen G R, Bewley D K, Field S B and Parnell C J 1966 The effect of oxygen on impairment of the proliferative capacity of human cells in culture by ionizing radiations of different LET *Int. J. Radiat. Biol. Relat. Stud. Phys. Chem. Med.* **10** 317–27
- Bedford J S and Mitchell J B 1973 Dose-rate effects in synchronous mammalian cells in culture *Radiat. Res.* **54** 316–27
- Brechbiel M W 2007 Targeted  $\alpha$ -therapy: past, present, future? *Dalton Trans.* **21** 4918–28
- Chérel M, Davodeau F, Kraeber-Bodéré F and Chatal J F 2006 Current status and perspectives in alpha radioimmunotherapy *Q J. Nucl. Med. Mol. Imaging* **50** 322–9
- Cooks T, Arazi L, Efrati M, Schmidt M, Marshak G, Kelson I and Keisari Y 2009a Interstitial wires releasing diffusing alpha emitters combined with chemotherapy improved local tumor control and survival in squamous cell carcinoma-bearing mice *Cancer* **115** 1791–801
- Cooks T, Arazi L, Schmidt M, Marshak G, Kelson I and Keisari Y 2008 Growth retardation and destruction of experimental squamous cell carcinoma by interstitial radioactive wires releasing diffusing alpha-emitting atoms *Int. J. Cancer* **122** 1657–64
- Cooks T, Schmidt M, Bittan H, Lazarov E, Arazi L, Kelson I and Keisari Y 2009b Local control of lung derived tumors by diffusing alpha-emitting atoms released from intratumoral wires loaded with radium-224 *Int. J. Radiat. Oncol. Biol. Phys.* **74** 966–73
- Couturier O, Supiot S, Degraef-Mouglin M, Faivre-Chauvet A, Carlier T, Chatal J F, Davodeau F and Cherel M 2005 Cancer radioimmunotherapy with alpha-emitting nuclides *Eur. J. Nucl. Med. Mol. Imaging* **32** 601–14
- Goodhead D T 1999 Mechanisms for the biological effectiveness of high-LET radiations *J. Radiat. Res. (Tokyo)* **40** Suppl 1–13
- Hall E J 1994 *Radiobiology for the Radiologist* 4th edn (Philadelphia, PA: Lippincott-Raven)
- ICRP 1984 Nonstochastic effects of ionizing radiation *ICRP Publication 41 (Ann. of the ICRP vol 14)* (Oxford: Pergamon)
- ICRP 1989 RBE for deterministic effects *ICRP Publication 58 (Ann. of the ICRP vol 20)* (Oxford: Pergamon)
- ICRP 1993 Age-dependent doses to members of the public from intake of radionuclides: part 2. Ingestion dose coefficients *ICRP Publication 67 (Ann. of the ICRP vol 23)* (Oxford: Pergamon)
- ICRP 2002 Basic anatomical and physiological data for use in radiological protection: reference values *ICRP Publication 89 (Ann. of the ICRP vol 32)* (Oxford: Pergamon)
- Jurcic J G *et al* 2002 Targeted alpha particle immunotherapy for myeloid leukemia *Blood* **100** 1233–9
- Jurcic J G 2005 Immunotherapy for acute myeloid leukemia *Curr. Oncol. Rep.* **7** 339–46
- Kennel S J, Boll R, Stabin M, Schuller H M and Mirzadeh S 1999 Radioimmunotherapy of micrometastases in lung with vascular targeted  $^{213}\text{Bi}$  *Br. J. Cancer* **80** 175–84
- Kneifel S *et al* 2006 Local targeting of malignant gliomas by the diffusible peptidic vector 1,4,7,10-tetraazacyclododecane-1-glutaric acid-4,7,10-triacetic acid-substance p *Clin. Cancer Res.* **12** 3843–50
- Leggett R W 1993 An age-specific kinetic model of lead metabolism in humans *Environ. Health Perspect.* **101** 598–616
- Mulford D A, Scheinberg D A and Jurcic J G 2005 The promise of targeted alpha-particle therapy *J. Nucl. Med.* **46** (Suppl.) 199S–204S
- Schmidt D *et al* 2004 Phase I clinical study on alpha-therapy for non Hodgkin lymphoma *Proc. 4th Alpha-immunotherapy Symp. (Düsseldorf, Germany, June 28–29)* ed A Morgenstern
- Stabin M G 2006 Nuclear medicine dosimetry *Phys. Med. Biol.* **51** R187–202
- Stabin M G 2009 OLINDA/EXM 1.1 (computer code documentation)

- Stabin M G and Siegel J A 2003 Physical models and dose factors for use in internal dose assessment *Health Phys.* **85** 294–310
- Stabin M G, Sparks R B and Crowe E 2005 OLINDA/EXM: the second-generation personal computer software for internal dose assessment in nuclear medicine *J. Nucl. Med.* **46** 1023–7
- Watchman C J, Jokisch D W, Patton P W, Rajon D A, Sgouros G and Bolch W E 2005 Absorbed fractions for alpha-particles in tissues of trabecular bone: considerations of marrow cellularity within the ICRP reference male *J. Nucl. Med.* **46** 1171–85
- Zalutsky M R 2006 Targeted alpha-particle therapy of microscopic disease: providing a further rationale for clinical investigation *J. Nucl. Med.* **47** 1238–40